Depletion of essential isoprenoids and ER stress induction following acute liver-specific deletion of HMG-CoA Reductase

Marco De Giorgi[1], Kelsey E. Jarrett[1,2], Jason C. Burton[1,2], Alexandria M. Doerfler[1], Ayrea Hurley[1], Ang Li[3], Rachel H. Hsu[1], Mia Furgurson[1], Kalyani R. Patel[4], Jun Han[5], Christoph H. Borchers[5,6,7,8], William R. Lagor[1*]

[1]Department of Molecular Physiology and Biophysics, Baylor College of Medicine, Houston, Texas, USA.

[2]Integrative Molecular and Biomedical Sciences Graduate Program, Baylor College of Medicine, Houston, Texas, USA.

[3]Department of Bioengineering, Rice University, Houston, Texas, USA.

[4]Department of Pathology, Texas Children's Hospital, Houston, Texas, USA.

[5]University of Victoria, Genome British Columbia Proteomics Centre, Victoria, British Columbia, Canada.

[6]Department of Data Intensive Science and Engineering, Skolkovo Institute of Science and Technology, Skolkovo Innovation Center, Moscow, Russia.

[7]Proteomics Centre, Segal Cancer Centre, Lady Davis Institute, Jewish General Hospital, McGill University, Montreal, Quebec, Canada.

[8]Gerald Bronfman Department of Oncology, Jewish General Hospital, Montreal, Quebec, Canada.

*To whom correspondence should be addressed

Corresponding author's contact information:

William R. Lagor, Ph.D.

Molecular Physiology and Biophysics Department

Baylor College of Medicine, Mail stop BCM 335

Houston, TX 77030

Phone: 713-798-8666

Email: lagor@bcm.edu

Running title: ER stress following *Hmgcr* deletion in the liver

Abbreviations: Hmgcr, HMG-CoA reductase; SREBP-2, sterol regulatory element-binding protein 2; ER, endoplasmic reticulum; LSKO, liver-specific knockout; Dhdds, Dehydrodolichyl diphosphate synthase subunit; PDSS1 and 2, Prenyl diphosphate synthase 1 and 2; GC, genome copies; gRNA, guide RNA; Aat, Alpha-1 antitrypsin; DKO, double knockout; HLP, hybrid liver-specific promoter; ALT, alanine aminotransferase; ALP, alkaline phosphatase.

Abstract and keywords

HMG-CoA Reductase (Hmgcr) is the rate-limiting enzyme in the mevalonate pathway and is inhibited by statins. In addition to cholesterol, Hmgcr activity is also required for synthesizing non-sterol isoprenoids, such as dolichol, ubiquinone, farnesylated and geranylgeranylated proteins. Here, we investigated the effects of Hmgcr inhibition on non-sterol isoprenoids in the liver. We have generated new genetic models to acutely delete genes in the mevalonate pathway in the liver using AAV-mediated delivery of Cre-recombinase (AAV-*Cre*) or CRISPR/Cas9 (AAV-CRISPR). The genetic deletion of *Hmgcr* by AAV-*Cre* resulted in extensive hepatocyte apoptosis and compensatory liver regeneration. At the biochemical level, we observed decreased levels of sterols and depletion of the non-sterol isoprenoids, dolichol and ubiquinone. At the cellular level, *Hmgcr* null hepatocytes showed endoplasmic reticulum (ER) stress and impaired N-glycosylation. We further hypothesized that the depletion of dolichol, essential for N-glycosylation, could be responsible for ER stress. Using AAV-CRISPR, we somatically disrupted Dehydrodolichyl diphosphate synthase subunit (*Dhdds*), encoding a branch point enzyme required for dolichol biosynthesis. *Dhdds* null livers showed ER stress and impaired N-glycosylation, along with apoptosis and regeneration. Finally, the combined deletion of *Hmgcr* and *Dhdds* synergistically exacerbated hepatocyte ER stress. Our data show a critical role for mevalonate-derived dolichol in the liver, and suggest that dolichol depletion is at least partially responsible for ER stress and apoptosis upon potent Hmgcr inhibition.

Keywords: Cholesterol synthesis and regulation, Liver, Isoprenoids, Endoplasmic reticulum, animal models, HMG-CoA, AAV, Dolichol, Dhdds, CRISPR/Cas9

Introduction

HMG-CoA reductase (HMGCR) is the rate-limiting enzyme in the mevalonate pathway, which leads to the production of cholesterol (1). HMGCR is an integral glycoprotein localized in the endoplasmic reticulum (ER) and is the target of statins, the most widely used cholesterol lowering drugs in the world (2). Cholesterol biosynthesis is tightly regulated through multiple mechanisms. First, the expression of HMGCR and all other enzymes in the mevalonate pathway is transcriptionally activated by sterol regulatory element-binding protein 2 (SREBP-2), which is processed when ER sterol levels are low (3). Second, the translation of HMGCR protein is subject to feedback inhibition by cholesterol (4, 5) or other non-sterol isoprenoids (6). Third, HMGCR undergoes Insig-dependent ubiquitination and proteasomal degradation in conditions of high levels of sterols and the branch product geranylgeranyl pyrophosphate in the ER (7, 8), which has a substantial effect on the levels of the enzyme in the liver (9, 10). Lastly, HMGCR activity is regulated by AMP-activated protein kinase- (AMPK) mediated phosphorylation, which can decrease cholesterol biosynthesis in low energy conditions (11). Collectively, these and other regulatory mechanisms finely tune HMGCR activity to maintain cellular cholesterol levels within a narrow physiological window.

Germline deletion of *Hmgcr* is embryonic lethal in mice around E9.5, demonstrating the importance of the mevalonate pathway for normal growth and development. Interestingly, heterozygous mice appeared normal and showed unaffected cholesterol biosynthesis, due to compensatory upregulation of wild type allele (12). Since this initial study, *Hmgcr* has been conditionally deleted in a number of tissues including the adipose (13), T-cells (14), skeletal muscle (15), myeloid cells (16), and the liver (17). The liver-specific knockout (LSKO) model is of particular interest as this is the major site for whole body cholesterol synthesis in rodents (18), and is the target of the statin drugs. *Hmgcr* LSKO mice were generated by crossing floxed animals with the Albumin-*Cre* transgenic line. These animals developed hepatic steatosis with apoptosis, hypoglycemia, and eventually liver failure and death. Viability could be rescued by supplementation with high doses of mevalonate in the drinking water. The mechanism of liver injury was at least partially

attributed to impairment of H-Ras and Rac1 isoprenylation (17). This work demonstrates the necessity for Hmgcr in hepatocyte viability. However, it is important to note that deletion with Albumin-*Cre* is not instantaneous, but occurs gradually over a period of many weeks- *i.e.* 40% at birth, 75% at weaning, and complete at 6 weeks of age in one example (19). The gradual nature of *Cre* excision in this model allows ample time for physiological compensation, making it difficult to study direct effects.

In addition to cholesterol, the mevalonate pathway produces other important non-sterol isoprenoids- such as dolichol, ubiquinone, and farnesyl and geranylgeranyl anchors for protein prenylation. Depletion of these metabolites has been suggested to be responsible for some beneficial effects of statins (20), as well as rare adverse events (21). However, the degree to which these metabolites are reduced upon Hmgcr inhibition, and their relative importance for liver physiology is not well understood. Insight into the role of these metabolites could be gained through genetic deletion of enzymes that occupy important branch points from the direct route to cholesterol. Dehydrodolichyl diphosphate synthase subunit (DHDDS) is a branch point enzyme, which in complex with Nogo-B Receptor constitutes a Cis-prenyltransferase that catalyzes the first committed step in the synthesis of dolichol, a glycosyl carrier essential for the biosynthesis of N-linked glycoproteins (22-25). Prenyl diphosphate synthase 1 and 2 (PDSS1 and 2) are branch point enzymes that elongate the prenyl side-chain of ubiquinone, which acts as electron carrier in mitochondrial respiration (26). Likewise, farnesyltransferase and geranylgeranyltransferase-I are branch point transferases that catalyze the covalent attachment of either the C-15 isoprene farnesyl or the C-20 isoprene geranylgeranyl group to the C-terminal end of multiple proteins (27). These include the proteins of the Ras superfamily, which are involved in cell growth, differentiation, signaling and mobility (28).

Recombinant Adeno-associated viruses (AAV) are small non-integrating, non-enveloped, single-stranded DNA viruses that can deliver transgenes to the liver with high efficiency (29). AAV delivery of Cre recombinase is rapidly gaining popularity for inducible deletion of genes in the adult liver (30, 31). AAV can also be used to deliver the Clustered regularly interspaced short palindromic repeats

(CRISPR)/Cas9 genome editing system, which can directly disrupt genes, thus bypassing the need to generate new floxed mouse models (32, 33). Here, we used these tools to study the effects of mevalonate pathway inhibition on non-sterol isoprenoids and hepatocyte physiology. A new *Hmgcr* mouse model was produced through introduction of a floxed allele into the germline, which was used to generate LSKO mice with AAV-*Cre* delivery to adult mice. In *Hmgcr* KO livers, we found depletion of certain non-sterol isoprenoids, including dolichol and ubiquinone, along with ER stress-induced apoptosis and impairment of N-linked glycosylation. We demonstrate that inhibiting the dolichol biosynthetic pathway with AAV-CRISPR-mediated deletion of *Dhdds,* partially phenocopied the *Hmgcr* LSKO mice. Finally, the combined deletion of *Hmgcr* and *Dhdds* resulted in exacerbation of hepatocyte ER stress and liver injury. Altogether, our work identifies dolichol as a non-sterol isoprenoid essential for hepatocyte viability, which is sensitive to potent inhibition of the mevalonate pathway.

Material and methods

Animals. Male *C57BL/6J* mice were obtained from Jackson Laboratories. Mice harboring a "knockout first" allele for *Hmgcr*, *Hmgcr*$^{tm1a(KOMP)Wtsi}$ (referred as *Hmgcr* FRT-FLOX), were generated by the knockout mouse project (KOMP) at UC Davis. These mice were used for generating *Hmgcr* conditional mice harboring the exon 5 flanked by loxP sites (*Hmgcr*$^{fl/fl}$). Details are included in the supplemental data. Liver-specific deletion of *Hmgcr* was accomplished by delivery of Cre recombinase with AAV8 vectors and expression of Cre under the control of the hybrid liver-specific promoter (HLP) (34). Liver-specific deletion of *Dhdds* was performed by delivery of CRISPR/Cas9 genome editing system with AAV8 vectors and expression of Cas9 under the control of HLP promoter. AAV were diluted in 300 µl of sterile saline and intraperitoneally injected to 6 week old mice (2 or 5 × 10^{11} or 1 ×10^{12} genome copies (GC) per mouse). All treatment conditions were randomly allocated within each cage of mice at the time of injection. Mice were fasted 5 hours prior to injection and again before subsequent blood collections. Blood was collected via retro-orbital bleeding using heparinized Natelson collection tubes, and plasma was isolated by centrifugation at 10,000 g for 20 minutes at 4°C. Mice were allowed free access to food and water and maintained on a standard chow diet. All experiments were approved by the Baylor College of Medicine Institutional Animal Care and Use Committee (IACUC) and performed in accordance with institutional guidelines under protocol number AN-6243. Experimental schemes in the figures were created with BioRender.

Plasmid design and cloning. 1326-pAAV-HLP-CRE-2A-EGFP-WPRE-BGHpA and 1162-pAAV-HLP-EmGFP-SpA plasmids were produced by standard molecular biology techniques. A gRNA targeting the exon 5 of *Dhdds* was designed by manual inspection based on the presence of a canonical NNGRRT protospacer adjacent motif for *Staphylococcus aureus* Cas9 (SaCas9). Cloning of gRNA (GCAGATGCAGATCACCCAGGAC) was accomplished by annealing oligonucleotides (Sigma-Aldrich), and ligating into the BbsI site of 1313-pAAV-U6-SA-BbsI-MluI-gRNA-HLP-SaCas9-HA-OLLAS-spA

(Addgene 109314) (35), to obtain 1560-pAAV-U6-SA-m*Dhdds*-gRNA2-HLP-SaCas9-HA-OLLAS-spA. Complete plasmid sequences are included in the supplemental data.

AAV production. Recombinant AAV8 vectors were generated as previously described (36) with several modifications (33). Plasmids required for AAV packaging, adenoviral helper plasmid pAdDeltaF6 (PL-F-PVADF6) and AAV8 packaging plasmid pAAV2/8 (PL-T-PV0007) were obtained from the University of Pennsylvania Vector Core. Each AAV transgene construct was co-transfected with the packaging constructs into 293T cells (ATCC, CRL-3216) using polyethylenimine. Cell pellets were harvested and purified using a single cesium chloride density gradient centrifugation. Fractions containing AAV were pooled and then dialyzed against PBS using a 100kD Spectra-Por® Float-A-Lyzer® G2 dialysis device (Spectrum Labs) to remove the cesium chloride. Purified AAV were concentrated using a Sartorius™ Vivaspin™ Turbo 4 Ultrafiltration Unit and stored at -80°C until use. AAV titers were calculated after DNase digestion using qPCR relative to a standard curve of the transgene plasmid. Primers used for titer are included in supplemental Table S1.

DNA analysis. Genomic DNA was extracted from livers and peripheral tissues using the DNeasy Blood and Tissue kit (Qiagen). 100 ng of DNA were PCR amplified for detecting *Hmgcr* deletion with APEX TaqRed Master Mix (Apex Bioresearch Products). PCR products were separated by agarose gel electrophoresis. For detecting editing at the *Dhdds* locus, 100 ng of DNA were PCR amplified with Phusion DNA polymerase (Roche) and the 680 bp product was separated by agarose gel electrophoresis and gel extracted using the QIAquick gel extraction kit (Qiagen). The PCR product was Sanger sequenced and the indel percentage was determined by Inference of CRISPR Edits (ICE) analysis (https://ice.synthego.com/#/) using a control chromatogram for comparison. For detecting AAV-genome integration events at the double-strand break site, 100 ng of DNA were PCR amplified with APEX TaqRed Master Mix (Apex Bioresearch Products) using a forward primer annealing upstream of the cut site in the *Dhdds* locus and a reverse primer specific for the viral inverted terminal repeat (ITR) sequence. The AAV-

CRISPR genome was PCR amplified using primers specific for the Cas9 sequence. All primers are listed in supplemental Table S1.

RNA analysis. RNA was isolated from liver and peripheral tissues using RNeasy Mini Kit (Qiagen). 1 µg of RNA was used for generating cDNA by the iScript cDNA synthesis kit (Bio-Rad). cDNA was diluted 1:25 and used as template for qPCR analysis using iTaq Universal SYBR Green Supermix (Bio-Rad) and ViiA 7 Real-Time PCR System (Thermo Fisher Scientific). A dissociation curve was carried out at the end of qPCR for assessing the homogeneity of the PCR products. Relative gene expression was calculated using the ΔΔCt method and graphed as fold change relative to TATA-Box Binding Protein (*Tbp*). All primers are listed in supplemental Table S1.

Western blot. Liver and most of the peripheral tissues were homogenized in ~10 volumes of RIPA buffer (50 mM Tris pH 8.0, 1 mM EDTA, 1% Triton X-100, 0.1% sodium dodecyl sulfate, 0.5% sodium deoxycholate, 150 mM sodium chloride, and protease inhibitors (Roche)) using a Bead Blaster 24 (Benchmark). Gastrocnemius, diaphragm and heart tissues were homogenized in ~10 volumes of RIPA buffer using a Polytron PT2100 homogenizer (Kinematica). For membrane fraction isolation, ~100 mg of liver samples were homogenized in 0.5 ml of lysing buffer (PBS supplemented with protease inhibitors) and centrifuged for discarding nuclei and cell debris. Supernatants were centrifuged at 57,000 g for 1 hour at 4°C, using a OPTIMA TLX ultracentrifuge with a Beckman TLA 100.3 rotor. Pellets (membrane fraction) were resuspended in 0.2 ml of lysing buffer. Protein concentrations were determined using BCA assay (Thermo-Pierce). Liver and peripheral tissue lysates (30 - 50 µg) or plasma (1 µl) were diluted in 4x LDS buffer (Life Technologies) supplemented with 5% beta-mercaptoethanol and separated by SDS-PAGE using 4-12% gradient gels (Life Technologies). Proteins were transferred to PVDF membranes (Millipore) followed by blocking for 2 hours at room temperature in a 2:1 solution of Odyssey Blocking Buffer (Li-Cor) and PBS with 0.05% Tween-20 (PBS-T). Primary antibodies were diluted in 1% BSA in PBS-T and

membranes were incubated overnight at 4°C. Secondary antibodies were incubated at room temperature for 1 hour and imaged using an Odyssey Classic (Li-Cor). All antibodies are listed in supplemental Table S2.

Immunohistochemistry. Livers were formalin-fixed for 24 hours, then gradually dehydrated with ethanol and paraffin-embedded. Immunohistochemistry and hematoxylin and eosin staining were performed by the Texas Digestive Diseases Morphology Core at Baylor College of Medicine, following standard protocols. Briefly, liver sections were deparaffinized and subjected to antigen retrieval with Target Retrieval Solution (DAKO). The sections were then incubated with 3% hydrogen peroxide, followed by incubation in normal serum to block nonspecific protein binding. Sections were incubated 1 hour at room temperature with anti-Ki67 (1:60, CRM325, Biocare). The Ki67 antibody was then detected with a Rabbit-on-Rodent HRP-Polymer (RMR622H, Biocare) and visualized with DAB chromogen (DB801, Biocare). TUNEL stainings were performed and detected using ApopTag Peroxidase In Situ Apoptosis Detection Kit (Millipore, S7100). All slides were counterstained with hematoxylin, dehydrated, and mounted with a permanent mounting medium. A Nikon Ci-L bright field microscope was used for imaging at the Integrated Microscopy Core (Baylor College of Medicine). Ki67- and TUNEL-positive cells quantification was performed by manual count of positive hepatocytes in five 200x magnification images per liver taken across the whole section. Section area was quantified using ImageJ24 (https://imagej.nih.gov/ij/).

Transmission electron microscopy (TEM). Livers were fixed in glutaraldehyde and processed for TEM at the Texas Digestive Diseases Morphology Core at Baylor College of Medicine.

Lipidomics. Sterols, isoprenyl phosphates and isoprenoids were extracted from ~150 mg of liver samples. Sterols were analyzed as previously described (37) with some modifications. Lipidomics analyses were conducted at the Genome British Columbia Proteomics Centre, University of Victoria, Canada. A detailed method for lipidomics is available in the supplemental data.

Plasma analyses. Alanine aminotransferase (ALT) activity was measured using the Teco ALT (SGPT) Kinetic Liquid Kit. Alkaline phosphatase (ALP) activity was measured using the Alkaline Phosphatase Assay Kit (Colorimetric) (ab83369, Abcam). Total cholesterol was measured using the Wako Cholesterol E kit. Triglycerides were measured using the Infinity Triglycerides Reagent (Thermo Fisher). As control of impaired glycosylation, plasma samples were enzymatically deglycosylated using Protein Deglycosylation Kit II (NEB).

Cell treatments. NIH3T3 cells (CRL-1658, ATCC) were cultured in DMEM (Fisher Scientific) supplemented with 10% fetal bovine serum (Sigma-Aldrich) and 1% penicillin/streptomycin (VWR), at 37°C and 5% CO_2. Cells were treated with 10 μM of farnesyltransferase inhibitor FTI-277 trifluoroacetate salt (Sigma-Aldrich) or 30 μM of geranylgeranyltransferase-I inhibitor GGTI 298 TFA salt (Selleckchem) for 48 hours, or 30 μM Lovastatin (Sigma-Aldrich) for 24 hours.

Statistics. All data are shown as the mean +/- standard deviation. Comparisons involving two groups were evaluated by a two-tailed student's t-test. For comparisons involving three or more groups, a one-way ANOVA was applied, with Tukey's post-test used to test for significant differences among groups. In all cases, significance was assigned at $p<0.05$.

Results

Efficient deletion of *Hmgcr* in the liver by AAV-*Cre*.

We sought to develop a novel genetic model of acute deletion of *Hmgcr* in the livers of adult mice. To this end, we first generated *Hmgcr*$^{+/-}$ mice harboring the nonfunctional *Hmgcr* FRT-FLOX allele by ES cell-mediated gene transfer (supplemental Fig. S1A). No *Hmgcr*$^{-/-}$ mice were born from *Hmgcr*$^{+/-}$ × *Hmgcr*$^{+/-}$ breeding pairs (supplemental Fig. S1B), confirming early embryonic lethality following complete disruption of *Hmgcr* (12). Then this line was crossed with FLP-transgenic mice and backcrossed to the *C57BL/6J* background, finally resulting in the generation of a mouse line harboring the exon 5 of *Hmgcr* flanked by loxP sites (*Hmgcr*$^{fl/fl}$) (Fig. 1A). To delete *Hmgcr* in the liver, we injected *Hmgcr*$^{fl/fl}$ mice with an AAV8 vector encoding the Cre Recombinase under the control of the liver-specific HLP promoter (Fig. 1A-B). At 2 weeks post-injection, *Hmgcr* LSKO mice showed the *Hmgcr* null allele in the liver (Fig. 1C), with no genetic deletion detected in any of the peripheral tissues analyzed (supplemental Fig. S2). *Hmgcr* mRNA level was found significantly decreased in livers from *Hmgcr* LSKO mice compared to control mice (Fig. 1D). Moreover, the deletion of *Hmgcr* resulted in transcriptional upregulation of Srebp-2-targeted genes of the mevalonate pathway (Fig. 1E-F), but not in any of the peripheral tissues analyzed (supplemental Fig. S3).

Hmgcr deletion results in depletion of sterol and non-sterol isoprenoids in the liver.

Next, we aimed to investigate the effects of *Hmgcr* deletion on the metabolites in the mevalonate pathway, with particular interest in the non-sterol isoprenoids (Fig. 2A). We used a targeted lipidomics approach for simultaneously measuring selected sterol and non-sterol isoprenoids. Livers from *Hmgcr* LSKO mice showed an overall decrease of cholesterol and sterol isoprenoids as compared to control mice (Fig. 2B). In terms of non-sterol isoprenoids, *Hmgcr* KO livers showed lower levels of dolichols and ubiquinones compared to control mice (Fig. 2C-D), with dolichol-18 and ubiquinone 9 being respectively the most abundant species in mice. No changes were observed in plasma total cholesterol and triglycerides

levels (supplemental Fig. S4). Together, these data show that the deletion of *Hmgcr* results in depletion of both sterols and important non-sterol isoprenoids in the liver.

Hmgcr LSKO mice show transient liver injury and regeneration.

Chronic deletion of *Hmgcr* in the liver was reported to cause severe liver damage and eventually liver failure (17). We investigated the effects of acute *Hmgcr* deletion on liver pathophysiology in our model. *Hmgcr* KO livers showed altered histology, characterized by enlarged and dying hepatocytes (Fig. 3A). This resulted in significant increases in plasma ALT and ALP levels as compared to control mice (Fig. 3B-C). Many hepatocytes died by apoptosis as shown by positive TUNEL staining in Fig. 3D-E. We also observed a massive burst of proliferating hepatocytes by Ki67 staining at this time point (Fig. 3F-G). Hepatocyte apoptosis gradually decreased at 4 and 8 weeks post AAV-*Cre* injection (supplemental Fig. S5). When we looked at our model at longer time points, we noticed a progressive loss of the *Hmgcr* null allele as well as enrichment of the *Hmgcr* floxed allele over time (Fig. 3H), indicating selective expansion of cells that escaped complete *Hmgcr* deletion. In contrast to previous work (17), the viability of the mice was not adversely affected by the loss of *Hmgcr* in the liver. Overall, these data show that the deletion of *Hmgcr* results in transient hepatocyte apoptosis followed by compensatory liver regeneration.

Hmgcr LSKO mice show hepatocyte ER stress-induced apoptosis and impaired N-linked glycosylation.

To further investigate the nature of liver injury, we performed a TEM analysis of livers following *Hmgcr* deletion (Fig. 4A). We observed swollen mitochondria and nucleus fragmentation as common features of apoptosis in *Hmgcr* KO hepatocytes (supplemental Table S3). Most importantly, we detected evidence of ER swelling (Fig. 4A and supplemental Table S3), which is commonly observed in conditions of ER stress (38). In parallel, we observed induction of the ER stress marker, Chop, and the apoptosis marker, Bax, in liver lysates from *Hmgcr* LSKO mice (Fig. 4B-C). Given the importance of dolichyl-phosphate for N-linked glycosylation in the ER (22), we hypothesized an ongoing impairment of the N-

linked glycosylation process in *Hmgcr* KO livers. To test this, we used western blot for analyzing the gel mobility of alpha-1 antitrypsin (Aat), which harbors three N-glycosylation sites (39). We observed decreased levels of mature (fully glycosylated) Aat in liver lysates as well as plasma from *Hmgcr* LSKO mice regardless the dose of AAV-*Cre* used for deleting *Hmgcr* (Fig. 4D-F). The previously described *Hmgcr* LSKO model showed impairment of protein prenylation (17). In our model, we found that the farnesylation of Prelamin-A was not impaired in *Hmgcr* KO livers even when five-fold higher dose of AAV-*Cre* was used (supplemental Fig. S6A-B). On the contrary, the geranylgeranylation of RhoA was impaired in *Hmgcr* KO livers only upon injection of the highest dose of AAV-*Cre*, resulting in the abnormal accumulation of RhoA in the cytosol (supplemental Fig. S6C-D). Together, these data show that the deletion of *Hmgcr* results in hepatocyte ER stress-induced apoptosis and impaired N-linked glycosylation.

***Dhdds* LSKO mice show hepatocyte ER-stress induced apoptosis and impaired N-linked glycosylation.**

Next, we hypothesized that the depletion of newly synthesized dolichyl phosphate could be responsible for the ER stress-induced apoptosis observed in *Hmgcr* KO livers (Fig. 2 and 4). We used the AAV-CRISPR system to somatically delete *Dhdds*, which is a branch point enzyme of the mevalonate pathway that, in complex with Nogo-B receptor, catalyzes the first committed step of dolichol biosynthesis (22). We injected mice with AAV-CRISPR or AAV-GFP (control) and collected liver and plasma samples at 2 and 4 weeks post-injection (Fig. 5A). AAV-CRISPR treatment resulted in the liver-restricted SaCas9 expression by the HLP promoter and efficient indel formation in exon 5 of *Dhdds* (supplemental Fig. S7), which was accompanied by a significant decrease of hepatic *Dhdds* mRNA levels (Fig. 5B). No detectable *Dhdds* editing was observed in any of the peripheral tissues analyzed (supplemental Fig. S8). The livers from *Dhdds* LSKO mice showed severe hepatocyte apoptosis and regeneration at 4 weeks post injection (Fig. 5C-F). Most importantly, we observed a large induction of Chop along with increased levels of Bax in livers from *Dhdds* LSKO mice (Fig. 5G-H). However, the observed liver damage was not reflected by significant elevation of ALT or ALP in plasma (supplemental Fig. S9), contrary to what was observed in

Hmgcr LSKO mice (Fig. 3). We next tested whether the deletion of *Dhdds* would result in impairment of N-linked glycosylation. Although there were not obvious differences in hepatic Aat levels (Fig. 5I), we found decreased levels of mature (fully glycosylated) Aat in plasma from *Dhdds* LSKO mice, along with a band of lower molecular weight at 4 weeks post-injection (Fig. 5J-K), suggesting impairment of N-glycosylation and processing. When we looked at the effects of *Dhdds* editing at a longer time point (6 weeks), we found that *Dhdds* mRNA levels had returned to normal with no evidence of increased ER stress or N-glycosylation impairment (supplemental Fig. S10), suggesting compensatory liver regeneration following the hepatocyte apoptosis observed at 4 weeks (Figure 5C-F). Overall, these data show that the liver-specific deletion of *Dhdds* results in transient hepatocyte ER stress-induced apoptosis and impaired N-linked glycosylation.

Combined deletion of *Hmgcr* and *Dhdds* exacerbates liver injury and hepatocyte ER stress.

We next tested if there is a genetic interaction between *Hmgcr* and *Dhdds* inhibition in regards to ER stress. We injected *Hmgcr*$^{fl/fl}$ mice with AAV-*Cre* and AAV-CRISPR in order to simultaneously delete *Hmgcr* and *Dhdds* in the liver (Double knockout mice (DKO); Fig. 6A). As controls, *Hmgcr*$^{fl/fl}$ mice were injected with either AAV-*Cre* or AAV-CRISPR alone. DKO mice showed efficient deletion of *Hmgcr,* along with CRISPR editing of *Dhdds,* which was readily detected by PCR for integration of the AAV genome at the cut site. Cre deletion and AAV-CRISPR editing resulted in significantly decreased levels of *Hmgcr* and *Dhdds* mRNA respectively (supplemental Fig. S11 and S12). We observed higher levels of ALT and ALP in plasma (Fig. 6B-C) as well as Chop in liver lysates from double knockout (DKO) mice as compared to *Hmgcr*- and *Dhdds* LSKO mice (Fig. 6D-E). These data show that further restriction of isoprenoid flux to dolichol synthesis via *Dhdds* disruption, acts synergistically with *Hmgcr* deletion to cause ER-stress induced apoptosis.

Discussion

Here, we report a new *Hmgcr* LSKO mouse model and its effects on isoprenoid metabolism and liver physiology. In contrast to the previous Albumin-*Cre* model, acute deletion of *Hmgcr* in the livers of adult mice is not lethal. Loss of *Hmgcr* results in transient liver injury characterized by hepatocyte apoptosis and compensatory liver regeneration. Livers from *Hmgcr* LSKO mice show depletion of important non-sterol isoprenoids, dolichol and ubiquinone, along with ER stress and defective N-linked glycosylation. We show that AAV-CRISPR-mediated deletion of *Dhdds* phenocopies the loss of *Hmgcr* in regards to ER stress and impaired N-linked glycosylation. Finally, further restriction of metabolic flux to dolichol, via the combined deletion of *Hmgcr* and *Dhdds,* synergistically exacerbates ER stress and liver injury.

The previously described Albumin-*Cre Hmgcr* deletion model resulted in liver failure and eventually death. Interestingly, cholesterol biosynthesis was only modestly affected, whereas protein isoprenylation was shown to be impaired, suggesting a direct role for prenylation defects in the liver failure (17). However, this phenotype may be consequence of chronic deficiency of Hmgcr since birth and potentially biased by adaptation mechanisms and compensatory changes. Moreover, it is reasonable to speculate that other non-sterol isoprenoids would also have been depleted at the time point of analysis. Here, we found that the acute deletion of *Hmgcr* in the liver resulted in depletion of dolichol and ubiquinone, suggesting that these non-sterol isoprenoids are particularly sensitive to potent mevalonate pathway inhibition. In contrast to the findings of Nagashima et al. (17), we did not observe major effects on protein prenylation. In fact, we observed accumulation of RhoA in liver cytosolic fractions as marker of geranylgeranylation impairment (40) only after delivery of a 5-fold higher AAV-*Cre* dose, whereas Prelamin-A farnesylation was never affected. Therefore, our data suggest that protein prenylation is not the branch product that is most sensitive to Hmgcr inhibition in the liver, and unlikely to account for hepatocyte apoptosis and liver injury. T-cells and myeloid cells have been reported to be more sensitive to the effects

of *Hmgcr* deletion or high-dose statins on prenylation of the Ras superfamily, possibly reflecting cell-specific differences in enzymatic activities or availability of their protein substrates (14, 16, 41).

Dolichol is a branch point product of the mevalonate pathway produced from farnesyl pyrophosphate. DHDDS and Nogo-B receptor form a Cis-prenyltransferase that catalyzes the first committed step of dolichol biosynthesis, connecting the mevalonate pathway to N-linked glycosylation (23-25). Newly synthesized dolichyl-phosphates are converted to dolichol-linked oligosaccharides required for N-linked glycosylation (22). Defects in the dolichol oligosaccharide assembly pathway or accumulation of hypoglycosylated misfolded glycoproteins cause a chronic induction of the unfolded protein response pathway and ER stress (42). In *Hmgcr* KO livers, we noticed hepatocyte ER stress-induced apoptosis along with impairment of N-linked glycosylation. All these data suggested the depletion of dolichol could be responsible for this phenotype. We confirmed this hypothesis by inhibiting the synthesis of dolichol via genetic deletion of *Dhdds*. Indeed, we observed hepatocyte ER stress and apoptosis, along with impairment of N-linked glycosylation. These results are consistent with the marked induction of ER stress and impaired N-linked glycosylation observed in Nogo-B receptor mutant fibroblasts (23). Moreover, mutations of *DHDDS* in humans have been associated with inherited retinitis pigmentosa because of impaired glycosylation of opsin, and type I congenital disorders of glycosylation (43, 44). Finally, the synergistic effect on liver ER stress by the disruption of dolichol biosynthesis combined with the genetic-induced inhibition of Hmgcr, further demonstrates the importance of mevalonate-derived dolichol synthesis for hepatocytes. Besides N-linked glycosylation, other dolichol dependent modifications, such as O-mannosylation, C-mannosylation and glycosylphosphatidylinositol (GPI)-anchor modification, may also be impaired in our models. In this regard, the elevation of ALP activity in plasma of *Hmgcr* LSKO and DKO mice might be a direct result of liver damage, but could also be due to defective attachment of the GPI-anchor, which anchors ALP to the plasma membrane.

The Nogo-B receptor has recently been identified as a negative regulator of hepatic lipogenesis and liver X receptor alpha (LXRα) activity. Albumin-*Cre*-mediated deletion of the Nogo-B receptor in the liver resulted in increased levels of plasma triglycerides and hepatic steatosis. In this report, loss of Nogo-B receptor was accompanied by increased nuclear translocation of LXRα, activation of lipogenic gene expression, and lipid accumulation in hepatocytes (45). Given the known interaction of Nogo-B receptor with *Dhdds* (23, 24), it would be interesting to know if there is a direct connection between cis-prenyltransferase activity of this complex and hepatic lipogenesis. Liver-specific deletion of *Dhdds* using either floxed mice or AAV-CRISPR deletion could be useful in resolving this issue.

In *Hmgcr* KO livers, we also observed decreased levels of ubiquinone, a branch product that acts as electron carrier in the electron transport chain. Although we cannot fully exclude an effect of ubiquinone depletion on hepatocyte ER stress and apoptosis, several reports show that ubiquinone deficiency affects mainly brain and kidney. In humans, mutations in *PDSS1* and *PDSS2* have been respectively associated with neurological disorder and Leigh syndrome with nephropathy (46, 47). *Pdss2* mutant mice recapitulated the ubiquinone deficiency and kidney disease phenotype, with no extra-renal disease (26, 48). More importantly, the liver specific deletion of *Pdss2* resulted in depletion of ubiquinone, but no evidence of liver pathology (26, 49). Altogether, these reports suggest that the liver is not primarily affected by ubiquinone deficiency or may compensate for its depletion. For instance, the liver can scavenge the ubiquinone carried by circulating lipoproteins (50), perhaps at levels adequate to support normal mitochondrial respiration.

The acute *Hmgcr* LSKO model showed extensive hepatocyte death and liver regeneration. When we investigated the effects of *Hmgcr* deletion over time, we observed a progressive loss of the *Hmgcr* null allele, and a corresponding increase in the floxed allele. This is clear evidence for expansion of hepatocytes that escaped complete removal of *Hmgcr* with AAV-*Cre*. The dose of virus used (2×10^{11} GC) is sufficient to mediate complete excision in >99% of hepatocytes (30), so this is an excellent model to study acute effects. However, since AAV-*Cre* is non-integrating, the viral transgene is lost with cell division, essentially

allowing the liver to be repopulated with Hmgcr+ hepatocytes over time. It is also possible that some of the regenerating cells are not hepatocyte-derived, an event that can happen in very severe cases of liver injury (31). Regardless of the cellular source of the Hmgcr+ hepatocytes, there is sufficient metabolic capacity to protect these animals from liver failure. This is in direct contrast to the Albumin-*Cre* transgenic model, which showed a more severe phenotype and died at six weeks of age (17), which is expected for such an integrated transgene.For this reason, our study adds value to the current models, because it is a tractable system to inactivate mevalonate synthesis, while avoiding any confounding developmental compensation.

Here, we also show that AAV-CRISPR is an efficient genetic tool for deleting genes in the mevalonate pathway in the livers of adult mice, with the great advantage of bypassing the need to generate new floxed animals. Similar to the *Hmgcr* LSKO mice, our *Dhdds* LSKO model also showed transient hepatocyte apoptosis and liver regeneration, which resolved at a later time point. It is notable that *Dhdds* disruption did not cause equivalent liver damage to the *Hmgcr* LSKO and DKO mice, at least based on the lack of significant increases in ALT and ALP. This could be due to the different efficiency and kinetics of gene disruption between the AAV-*Cre* and the AAV-CRISPR systems. Optimization of gRNA design and vector dose may overcome these limitations. However, we also cannot exclude that different cell death mechanisms other than apoptosis may occur (i.e. necrosis) and differentially impact ALT elevations in the *Hmgcr* vs *Dhdds* KO mice. Finally, the depletion of other non-sterol isoprenoids may also contribute to the greater degree of liver damage observed in *Hmgcr* LSKO compared to *Dhdds* LSKO mice.

In conclusion, we report a genetic model to acutely inhibit the mevalonate pathway in the liver. We show that the deletion of *Hmgcr* results in depletion of non-sterol isoprenoids, dolichol and ubiquinone, and severe ER stress. We demonstrate that the genetic inhibition of dolichol biosynthesis partially mimics the liver phenotype observed in *Hmgcr* LSKO mice. Moreover, the combined inhibition of the mevalonate pathway and dolichol biosynthesis exacerbates liver injury and hepatocyte ER stress. Altogether, our data

show a critical role for mevalonate-derived dolichol in the liver, and suggest this metabolite could play an important role in mediating the effects of statins on liver physiology.

Data availability statement: All data are contained within the manuscript and supplemental file.

Acknowledgments/grant support: The authors thank Dr Stephen G Young, (UCLA) for providing anti Prelamin-A antibody. This work was supported by the National Institutes of Health (HL132840, DK124477 to W.R.L.; T32HL07676, T32GM08321 to K.E.J.; T32HL07676 to A.M.D. and R01-HL132840-02S1 to M.N.F.), the American Heart Association (19POST34430092 to M.D.G. and 19PRE34380467 to A.M.D.). This work was also supported by the Texas Digestive Diseases Morphology Core (P30DK56338) and the Integrated Microscopy Core (DK56338, and CA125123). The content is solely the responsibility of the authors and does not necessarily represent the official views of the National Institutes of Health.

References

1. Goldstein, J. L., and M. S. Brown. 1990. Regulation of the mevalonate pathway. *Nature* **343**: 425-430.

2. Silverman, M. G., B. A. Ference, K. Im, S. D. Wiviott, R. P. Giugliano, S. M. Grundy, E. Braunwald, and M. S. Sabatine. 2016. Association Between Lowering LDL-C and Cardiovascular Risk Reduction Among Different Therapeutic Interventions: A Systematic Review and Meta-analysis. *JAMA* **316**: 1289-1297.

3. Brown, M. S., and J. L. Goldstein. 1997. The SREBP pathway: regulation of cholesterol metabolism by proteolysis of a membrane-bound transcription factor. *Cell* **89**: 331-340.

4. Chambers, C. M., and G. C. Ness. 1998. Dietary cholesterol regulates hepatic 3-hydroxy-3-methylglutaryl coenzyme A reductase gene expression in rats primarily at the level of translation. *Arch Biochem Biophys* **354**: 317-322.

5. Ness, G. C., and C. M. Chambers. 2000. Feedback and hormonal regulation of hepatic 3-hydroxy-3-methylglutaryl coenzyme A reductase: the concept of cholesterol buffering capacity. *Proc Soc Exp Biol Med* **224**: 8-19.

6. Johnson, B. M., and R. A. DeBose-Boyd. 2018. Underlying mechanisms for sterol-induced ubiquitination and ER-associated degradation of HMG CoA reductase. *Semin Cell Dev Biol* **81**: 121-128.

7. Sever, N., T. Yang, M. S. Brown, J. L. Goldstein, and R. A. DeBose-Boyd. 2003. Accelerated degradation of HMG CoA reductase mediated by binding of insig-1 to its sterol-sensing domain. *Mol Cell* **11**: 25-33.

8. Schumacher, M. M., R. Elsabrouty, J. Seemann, Y. Jo, and R. A. DeBose-Boyd. 2015. The prenyltransferase UBIAD1 is the target of geranylgeraniol in degradation of HMG CoA reductase. *Elife* **4**.

9. Ness, G. C., C. M. Chambers, and D. Lopez. 1998. Atorvastatin action involves diminished recovery of hepatic HMG-CoA reductase activity. *J Lipid Res* **39**: 75-84.

10. Engelking, L. J., G. Liang, R. E. Hammer, K. Takaishi, H. Kuriyama, B. M. Evers, W. P. Li, J. D. Horton, J. L. Goldstein, and M. S. Brown. 2005. Schoenheimer effect explained--feedback regulation of cholesterol synthesis in mice mediated by Insig proteins. *J Clin Invest* **115**: 2489-2498.

11. Loh, K., S. Tam, L. Murray-Segal, K. Huynh, P. J. Meikle, J. W. Scott, B. van Denderen, Z. Chen, R. Steel, N. D. LeBlond, L. A. Burkovsky, C. O'Dwyer, J. R. C. Nunes, G. R. Steinberg, M. D. Fullerton, S. Galic, and B. E. Kemp. 2019. Inhibition of Adenosine Monophosphate-Activated Protein Kinase-3-Hydroxy-3-Methylglutaryl Coenzyme A Reductase Signaling Leads to Hypercholesterolemia and Promotes Hepatic Steatosis and Insulin Resistance. *Hepatol Commun* **3**: 84-98.

12. Ohashi, K., J. Osuga, R. Tozawa, T. Kitamine, H. Yagyu, M. Sekiya, S. Tomita, H. Okazaki, Y. Tamura, N. Yahagi, Y. Iizuka, K. Harada, T. Gotoda, H. Shimano, N. Yamada, and S. Ishibashi. 2003. Early embryonic lethality caused by targeted disruption of the 3-hydroxy-3-methylglutaryl-CoA reductase gene. *J Biol Chem* **278**: 42936-42941.

13. Yeh, Y. S., H. F. Jheng, M. Iwase, M. Kim, S. Mohri, J. Kwon, S. Kawarasaki, Y. Li, H. Takahashi, T. Ara, W. Nomura, T. Kawada, and T. Goto. 2018. The Mevalonate Pathway Is Indispensable for Adipocyte Survival. *iScience* **9**: 175-191.

14. Lacher, S. M., J. Bruttger, B. Kalt, J. Berthelet, K. Rajalingam, S. Wortge, and A. Waisman. 2017. HMG-CoA reductase promotes protein prenylation and therefore is indispensible for T-cell survival. *Cell Death Dis* **8**: e2824.

15. Osaki, Y., Y. Nakagawa, S. Miyahara, H. Iwasaki, A. Ishii, T. Matsuzaka, K. Kobayashi, S. Yatoh, A. Takahashi, N. Yahagi, H. Suzuki, H. Sone, K. Ohashi, S. Ishibashi, N. Yamada, and H. Shimano. 2015. Skeletal muscle-specific HMG-CoA reductase knockout mice exhibit rhabdomyolysis: A model for statin-induced myopathy. *Biochem Biophys Res Commun* **466**: 536-540.

16. Sakai, K., S. Nagashima, T. Wakabayashi, B. Tumenbayar, H. Hayakawa, M. Hayakawa, T. Karasawa, K. Ohashi, H. Yamazaki, A. Takei, S. Takei, D. Yamamuro, M. Takahashi, H. Yagyu, J. I. Osuga, M. Takahashi, S. I. Tominaga, and S. Ishibashi. 2018. Myeloid HMG-CoA (3-Hydroxy-3-

Methylglutaryl-Coenzyme A) Reductase Determines Atherosclerosis by Modulating Migration of Macrophages. *Arterioscler Thromb Vasc Biol* **38**: 2590-2600.

17. Nagashima, S., H. Yagyu, K. Ohashi, F. Tazoe, M. Takahashi, T. Ohshiro, T. Bayasgalan, K. Okada, M. Sekiya, J. Osuga, and S. Ishibashi. 2012. Liver-specific deletion of 3-hydroxy-3-methylglutaryl coenzyme A reductase causes hepatic steatosis and death. *Arterioscler Thromb Vasc Biol* **32**: 1824-1831.

18. Dietschy, J. M., S. D. Turley, and D. K. Spady. 1993. Role of liver in the maintenance of cholesterol and low density lipoprotein homeostasis in different animal species, including humans. *J Lipid Res* **34**: 1637-1659.

19. Postic, C., and M. A. Magnuson. 2000. DNA excision in liver by an albumin-Cre transgene occurs progressively with age. *Genesis* **26**: 149-150.

20. Oesterle, A., U. Laufs, and J. K. Liao. 2017. Pleiotropic Effects of Statins on the Cardiovascular System. *Circ Res* **120**: 229-243.

21. Ward, N. C., G. F. Watts, and R. H. Eckel. 2019. Statin Toxicity. *Circ Res* **124**: 328-350.

22. Wolfe, L. A., E. Morava, M. He, J. Vockley, and K. M. Gibson. 2012. Heritable disorders in the metabolism of the dolichols: A bridge from sterol biosynthesis to molecular glycosylation. *Am J Med Genet C Semin Med Genet* **160C**: 322-328.

23. Park, E. J., K. A. Grabinska, Z. Guan, V. Stranecky, H. Hartmannova, K. Hodanova, V. Baresova, J. Sovova, L. Jozsef, N. Ondruskova, H. Hansikova, T. Honzik, J. Zeman, H. Hulkova, R. Wen, S. Kmoch, and W. C. Sessa. 2014. Mutation of Nogo-B receptor, a subunit of cis-prenyltransferase, causes a congenital disorder of glycosylation. *Cell Metab* **20**: 448-457.

24. Grabinska, K. A., B. H. Edani, E. J. Park, J. R. Kraehling, and W. C. Sessa. 2017. A conserved C-terminal RXG motif in the NgBR subunit of cis-prenyltransferase is critical for prenyltransferase activity. *J Biol Chem* **292**: 17351-17361.

25. Grabinska, K. A., E. J. Park, and W. C. Sessa. 2016. cis-Prenyltransferase: New Insights into Protein Glycosylation, Rubber Synthesis, and Human Diseases. *J Biol Chem* **291**: 18582-18590.

26. Peng, M., M. J. Falk, V. H. Haase, R. King, E. Polyak, M. Selak, M. Yudkoff, W. W. Hancock, R. Meade, R. Saiki, A. L. Lunceford, C. F. Clarke, and D. L. Gasser. 2008. Primary coenzyme Q deficiency in Pdss2 mutant mice causes isolated renal disease. *PLoS Genet* **4**: e1000061.

27. Yang, S. H., S. Y. Chang, Y. Tu, G. W. Lawson, M. O. Bergo, L. G. Fong, and S. G. Young. 2012. Severe hepatocellular disease in mice lacking one or both CaaX prenyltransferases. *J Lipid Res* **53**: 77-86.

28. Wennerberg, K., K. L. Rossman, and C. J. Der. 2005. The Ras superfamily at a glance. *J Cell Sci* **118**: 843-846.

29. De Giorgi, M., and W. R. Lagor. 2019. Gene Delivery in Lipid Research and Therapies. *Methodist Debakey Cardiovasc J* **15**: 62-69.

30. Bauer, R. C., M. Sasaki, D. M. Cohen, J. Cui, M. A. Smith, B. O. Yenilmez, D. J. Steger, and D. J. Rader. 2015. Tribbles-1 regulates hepatic lipogenesis through posttranscriptional regulation of C/EBPalpha. *J Clin Invest* **125**: 3809-3818.

31. Pastore, N., T. Huynh, N. J. Herz, A. Calcagni, T. J. Klisch, L. Brunetti, K. H. Kim, M. De Giorgi, A. Hurley, A. Carissimo, M. Mutarelli, N. Aleksieva, L. D'Orsi, W. R. Lagor, D. D. Moore, C. Settembre, M. J. Finegold, S. J. Forbes, and A. Ballabio. 2020. TFEB regulates murine liver cell fate during development and regeneration. *Nat Commun* **11**: 2461.

32. Ran, F. A., L. Cong, W. X. Yan, D. A. Scott, J. S. Gootenberg, A. J. Kriz, B. Zetsche, O. Shalem, X. Wu, K. S. Makarova, E. V. Koonin, P. A. Sharp, and F. Zhang. 2015. In vivo genome editing using Staphylococcus aureus Cas9. *Nature* **520**: 186-191.

33. Jarrett, K. E., C. Lee, M. De Giorgi, A. Hurley, B. K. Gillard, A. M. Doerfler, A. Li, H. J. Pownall, G. Bao, and W. R. Lagor. 2018. Somatic Editing of Ldlr With Adeno-Associated Viral-CRISPR Is an Efficient Tool for Atherosclerosis Research. *Arterioscler Thromb Vasc Biol* **38**: 1997-2006.

34. McIntosh, J., P. J. Lenting, C. Rosales, D. Lee, S. Rabbanian, D. Raj, N. Patel, E. G. Tuddenham, O. D. Christophe, J. H. McVey, S. Waddington, A. W. Nienhuis, J. T. Gray, P. Fagone, F. Mingozzi, S. Z. Zhou, K. A. High, M. Cancio, C. Y. Ng, J. Zhou, C. L. Morton, A. M. Davidoff, and A. C. Nathwani.

2013. Therapeutic levels of FVIII following a single peripheral vein administration of rAAV vector encoding a novel human factor VIII variant. *Blood* **121**: 3335-3344.

35. Li, A., C. M. Lee, A. E. Hurley, K. E. Jarrett, M. De Giorgi, W. Lu, K. S. Balderrama, A. M. Doerfler, H. Deshmukh, A. Ray, G. Bao, and W. R. Lagor. 2019. A Self-Deleting AAV-CRISPR System for In Vivo Genome Editing. *Mol Ther Methods Clin Dev* **12**: 111-122.

36. Lagor, W. R., J. C. Johnston, M. Lock, L. H. Vandenberghe, and D. J. Rader. 2013. Adeno-associated viruses as liver-directed gene delivery vehicles: focus on lipoprotein metabolism. *Methods Mol Biol* **1027**: 273-307.

37. Tang, Z., and F. P. Guengerich. 2010. Dansylation of unactivated alcohols for improved mass spectral sensitivity and application to analysis of cytochrome P450 oxidation products in tissue extracts. *Anal Chem* **82**: 7706-7712.

38. Oslowski, C. M., and F. Urano. 2011. Measuring ER stress and the unfolded protein response using mammalian tissue culture system. *Methods Enzymol* **490**: 71-92.

39. McCarthy, C., R. Saldova, M. R. Wormald, P. M. Rudd, N. G. McElvaney, and E. P. Reeves. 2014. The role and importance of glycosylation of acute phase proteins with focus on alpha-1 antitrypsin in acute and chronic inflammatory conditions. *J Proteome Res* **13**: 3131-3143.

40. Berndt, N., and S. M. Sebti. 2011. Measurement of protein farnesylation and geranylgeranylation in vitro, in cultured cells and in biopsies, and the effects of prenyl transferase inhibitors. *Nat Protoc* **6**: 1775-1791.

41. Healy, A., J. M. Berus, J. L. Christensen, C. Lee, C. Mantsounga, W. Dong, J. P. Watts, Jr., M. Assali, N. Ceneri, R. Nilson, J. Neverson, W. C. Wu, G. Choudhary, and A. R. Morrison. 2020. Statins Disrupt Macrophage Rac1 Regulation Leading to Increased Atherosclerotic Plaque Calcification. *Arterioscler Thromb Vasc Biol* **40**: 714-732.

42. Cherepanova, N., S. Shrimal, and R. Gilmore. 2016. N-linked glycosylation and homeostasis of the endoplasmic reticulum. *Curr Opin Cell Biol* **41**: 57-65.

43. Zelinger, L., E. Banin, A. Obolensky, L. Mizrahi-Meissonnier, A. Beryozkin, D. Bandah-Rozenfeld, S. Frenkel, T. Ben-Yosef, S. Merin, S. B. Schwartz, A. V. Cideciyan, S. G. Jacobson, and D. Sharon. 2011. A missense mutation in DHDDS, encoding dehydrodolichyl diphosphate synthase, is associated with autosomal-recessive retinitis pigmentosa in Ashkenazi Jews. *Am J Hum Genet* **88**: 207-215.

44. Sabry, S., S. Vuillaumier-Barrot, E. Mintet, M. Fasseu, V. Valayannopoulos, D. Heron, N. Dorison, C. Mignot, N. Seta, I. Chantret, T. Dupre, and S. E. Moore. 2016. A case of fatal Type I congenital disorders of glycosylation (CDG I) associated with low dehydrodolichol diphosphate synthase (DHDDS) activity. *Orphanet J Rare Dis* **11**: 84.

45. Hu, W., W. Zhang, Y. Chen, U. Rana, R. J. Teng, Y. Duan, Z. Liu, B. Zhao, J. Foeckler, H. Weiler, R. E. Kallinger, M. J. Thomas, K. Zhang, J. Han, and Q. R. Miao. 2016. Nogo-B receptor deficiency increases liver X receptor alpha nuclear translocation and hepatic lipogenesis through an adenosine monophosphate-activated protein kinase alpha-dependent pathway. *Hepatology* **64**: 1559-1576.

46. Mollet, J., I. Giurgea, D. Schlemmer, G. Dallner, D. Chretien, A. Delahodde, D. Bacq, P. de Lonlay, A. Munnich, and A. Rotig. 2007. Prenyldiphosphate synthase, subunit 1 (PDSS1) and OH-benzoate polyprenyltransferase (COQ2) mutations in ubiquinone deficiency and oxidative phosphorylation disorders. *J Clin Invest* **117**: 765-772.

47. Lopez, L. C., M. Schuelke, C. M. Quinzii, T. Kanki, R. J. Rodenburg, A. Naini, S. Dimauro, and M. Hirano. 2006. Leigh syndrome with nephropathy and CoQ10 deficiency due to decaprenyl diphosphate synthase subunit 2 (PDSS2) mutations. *Am J Hum Genet* **79**: 1125-1129.

48. Quinzii, C. M., C. Garone, V. Emmanuele, S. Tadesse, S. Krishna, B. Dorado, and M. Hirano. 2013. Tissue-specific oxidative stress and loss of mitochondria in CoQ-deficient Pdss2 mutant mice. *FASEB J* **27**: 612-621.

49. Falk, M. J., E. Polyak, Z. Zhang, M. Peng, R. King, J. S. Maltzman, E. Okwuego, O. Horyn, E. Nakamaru-Ogiso, J. Ostrovsky, L. X. Xie, J. Y. Chen, B. Marbois, I. Nissim, C. F. Clarke, and D. L.

Gasser. 2011. Probucol ameliorates renal and metabolic sequelae of primary CoQ deficiency in Pdss2 mutant mice. *EMBO Mol Med* **3**: 410-427.

50. Tomasetti, M., R. Alleva, M. D. Solenghi, and G. P. Littarru. 1999. Distribution of antioxidants among blood components and lipoproteins: significance of lipids/CoQ10 ratio as a possible marker of increased risk for atherosclerosis. *Biofactors* **9**: 231-240.

Figures and figure legends

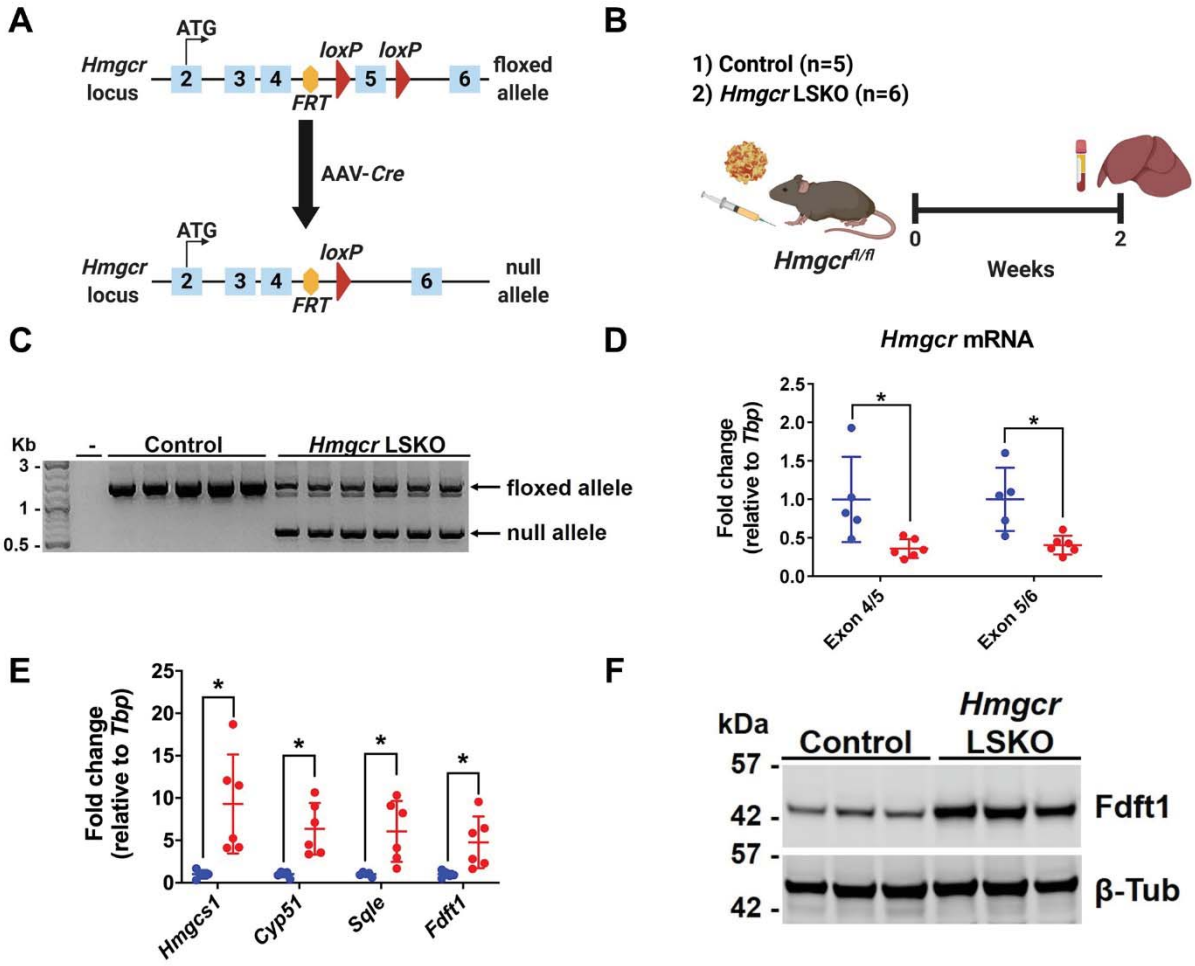

Figure 1. Efficient deletion of *Hmgcr* in the liver by AAV-*Cre*. (A) Schematic diagram of genetic deletion of *Hmgcr* (Exon 5) by AAV-*Cre* in the liver of *Hmgcr*$^{fl/fl}$ mice. (B) 6 week old *Hmgcr*$^{fl/fl}$ mice were injected with 2 × 10^{11} GC of AAV-*Cre* or AAV-GFP (control). 2 weeks post-injection, liver and plasma were collected for analyses. (C) Genotyping PCR on liver DNA showing two main bands corresponding to the *Hmgcr* floxed (1364 bp) and null (544 bp) alleles. Minus (-) indicates water only control. (D) qPCR analysis of *Hmgcr* mRNA levels in livers from control (blue) and *Hmgcr* LSKO (red) mice. (E) qPCR analysis of representative genes of the mevalonate pathway in the liver of *Hmgcr* LSKO (red) and control (blue) mice. (F) Western blot analysis of Fdft1 in liver lysates from *Hmgcr* LSKO and control mice, with β-Tubulin (β-Tub) used as a loading control. *Hmgcs1*: 3-Hydroxy-3-Methylglutaryl-CoA Synthase 1; *Cyp51*: Cytochrome P450 Family 51; *Sqle*: squalene epoxidase; *Fdft1*: farnesyl-diphosphate farnesyltransferase 1.

Data are shown as mean ± SD with significance determined by two-tailed student's t-test. n= 5 control and 6 *Hmgcr* LSKO mice. *p<0.05.

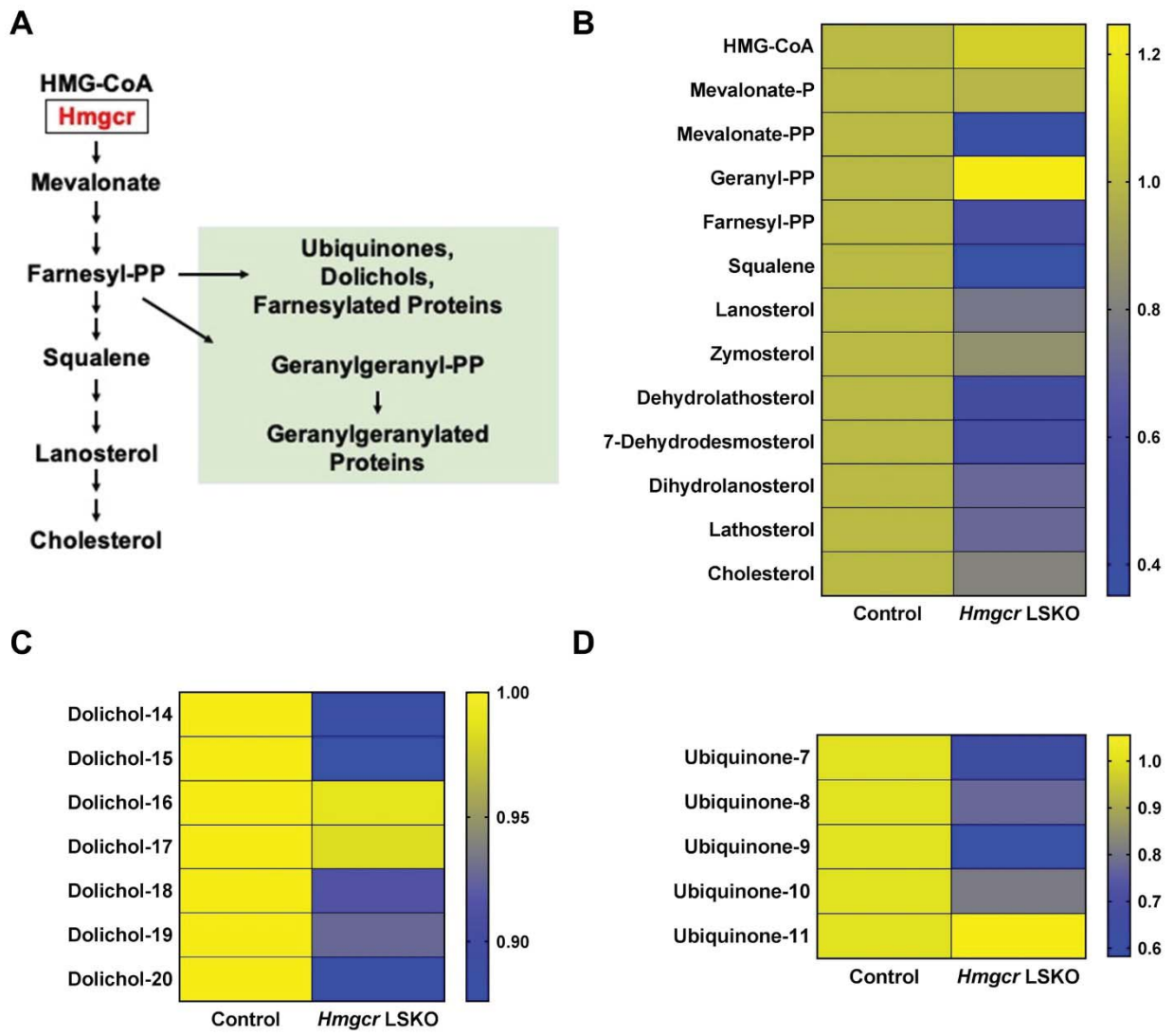

Figure 2. *Hmgcr* deletion results in depletion of sterol and non-sterol isoprenoids in the liver. (A) Schematic diagram of the mevalonate pathway and selected branch point products. Representative metabolites are shown. Non-sterol isoprenoids are shown in green. Heat maps showing sterol isoprenoids (B), dolichols (C) and ubiquinones (D) measured in livers from *Hmgcr* LSKO and control mice by a lipidomics approach. Data are presented as relative abundance of each metabolite in *Hmgcr* KO compared to control livers. n= 5 control and 6 *Hmgcr* LSKO mice.

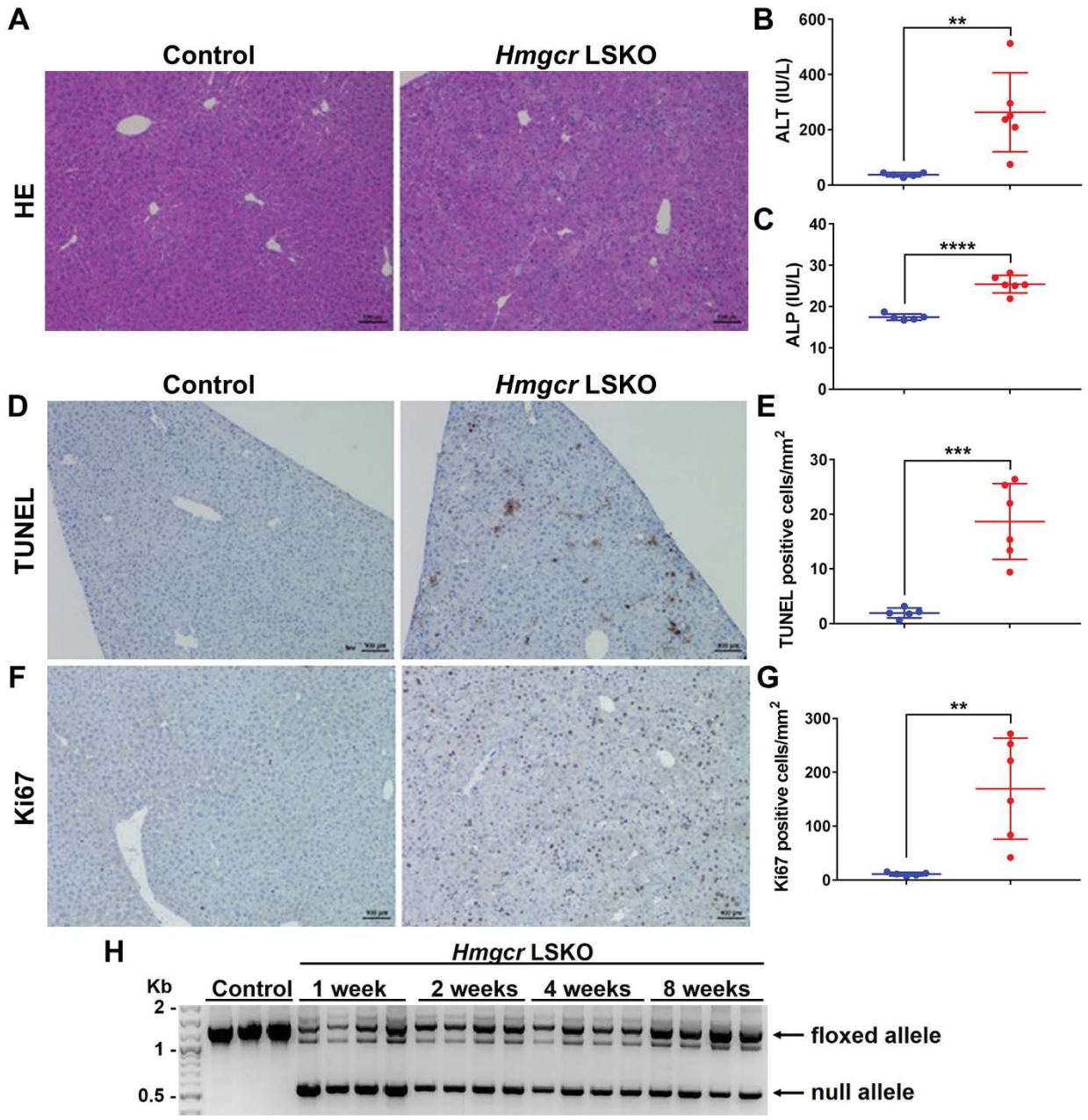

Figure 3. *Hmgcr* LSKO mice show increased hepatocyte apoptosis and liver regeneration. (A) Hematoxylin and eosin (HE) staining of control and *Hmgcr* KO liver sections. ALT (B) and ALP (C) measurement in plasma from control (blue) and *Hmgcr* LSKO (red) mice. (D) TUNEL staining of liver sections and (E) quantification of TUNEL-positive hepatocytes per mm^2 in control (blue) and *Hmgcr* KO (red) livers. (F) Ki67 staining of liver sections and (G) quantification of Ki67-positive hepatocytes per mm^2 in control (blue) and *Hmgcr* KO (red) livers. (H) *Hmgcr* genotyping PCR on liver DNA from *Hmgcr* LSKO

mice at 1, 2, 4 and 8 weeks post-AAV-*Cre* injection. The two main bands correspond to the *Hmgcr* floxed (1364 bp) and null (544 bp) alleles. Representative IHC images are shown (scale bar is 100 μm). Data are presented as mean ± SD, with significance determined by two-tailed student's t-test. n= 5 control and 6 *Hmgcr* LSKO mice. **p<0.01, ***p<0.001 and ****p<0.0001.

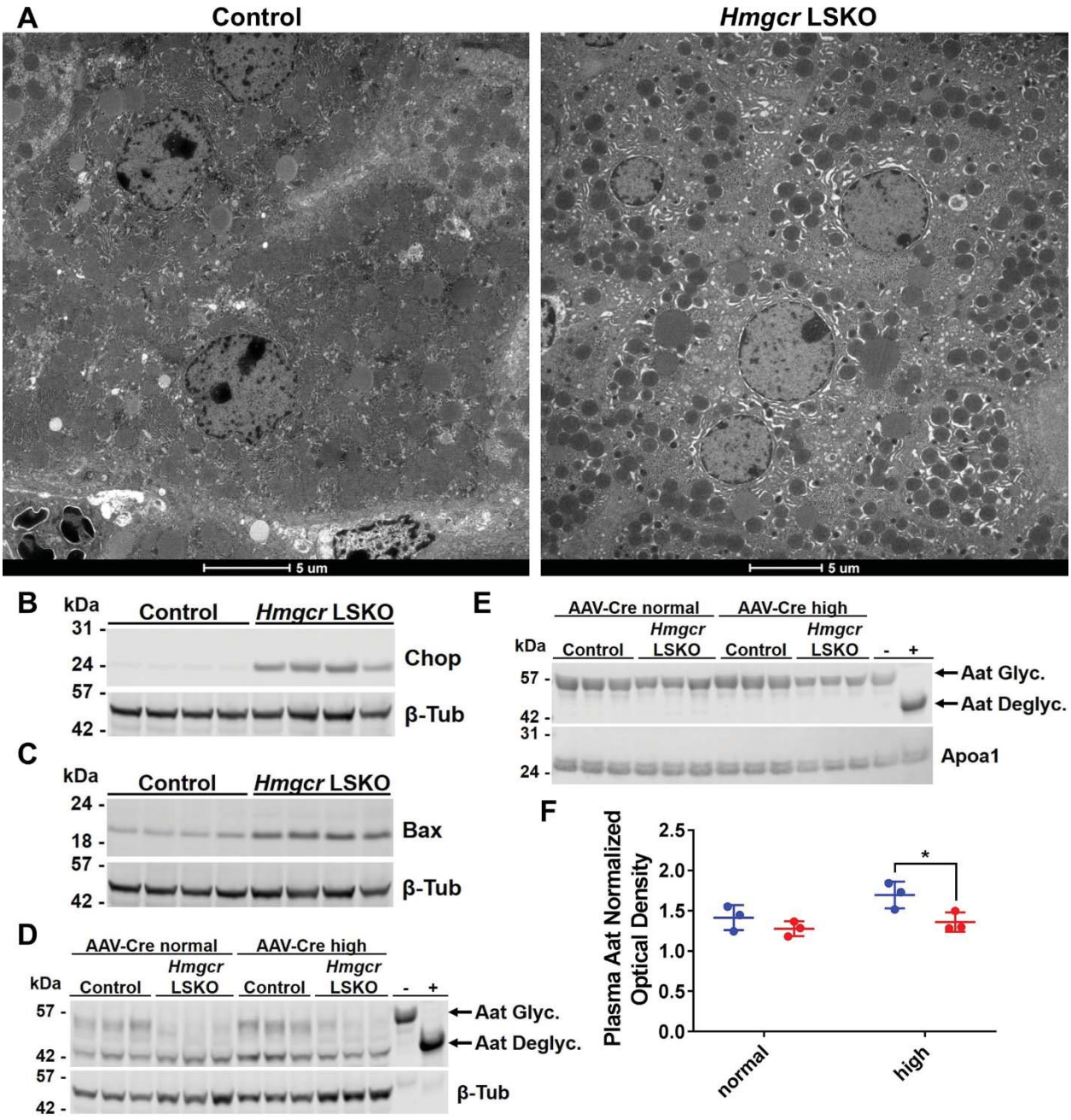

Figure 4. *Hmgcr* LSKO mice show hepatocyte ER stress-induced apoptosis and impaired N-glycosylation. (A) Representative TEM of hepatocytes in liver from control and *Hmgcr* LSKO mice. Scale bar is 5 μM. Western blot analysis of Chop (B), Bax (C) and Aat (D) in liver lysates from control and *Hmgcr* LSKO mice, with β-Tubulin used as a loading control. (E) Western blot analysis of Aat in plasma from control and *Hmgcr* LSKO mice, with Apoa1 used as a loading control. (F) Densitometry analysis of

plasma Aat in control (blue) and *Hmgcr* LSKO (red) mice. *Hmgcr* LSKO samples in (D) and (E) are from *Hmgcr*$^{fl/fl}$ mice injected with either 2×10^{11} (AAV-*Cre* normal) or 10^{12} (AAV-*Cre* high) GC of AAV-*Cre*. In panels (D) and (E), plasma was treated with an enzymatic deglycosylation kit (+) or sham (-) as control of the effect of glycosylation on protein mobility. "Aat Glyc": glycosylated (mature) Aat; "Aat Deglyc": deglycosylated Aat. Representative western blots are shown. Densitometry data are normalized to Apoa1 and shown as mean ± SD with significance determined by two-tailed student's t-test. n=3. *$p<0.05$.

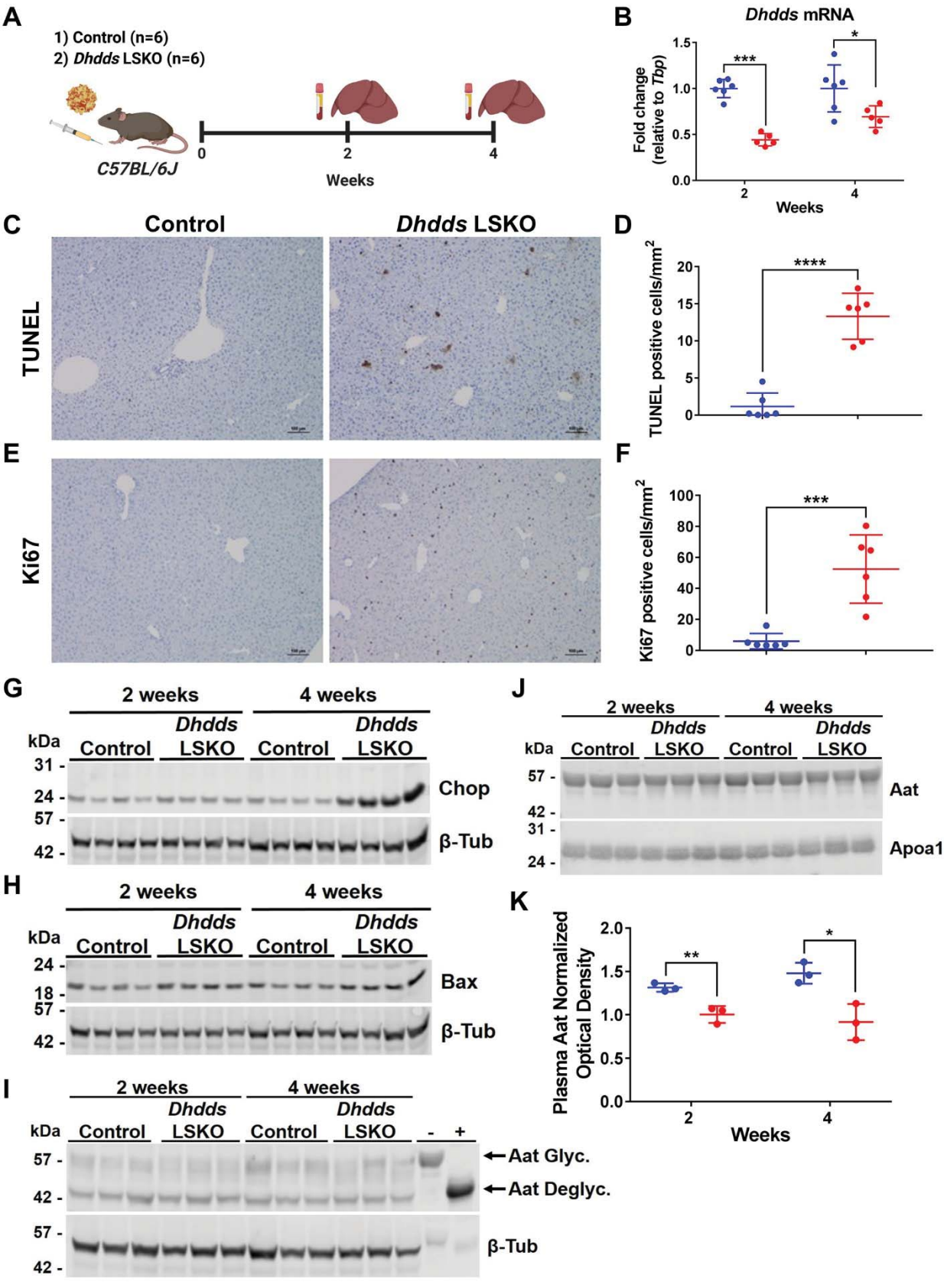

Figure 5. *Dhdds* LSKO mice show hepatocyte ER stress-induced apoptosis. (A) 6 week old *C57BL/6J* mice were injected with 5×10^{11} GC of AAV-CRISPR or AAV-GFP (control) and liver and plasma samples were collected at 2 and 4 weeks post-injection for analysis. (B) qPCR analysis of *Dhdds* mRNA levels in livers from control (blue) and *Dhdds* LSKO (red) mice. (C) TUNEL staining of liver sections and (D) quantification of TUNEL-positive hepatocytes per mm^2 in control (blue) and *Dhdds* LSKO (red) livers at 4 weeks post-injection. (E) Ki67 staining of liver sections and (F) quantification of Ki67-positive hepatocytes per mm^2 in control (blue) and *Dhdds* LSKO (red) livers at 4 weeks post-injection. Representative images from mice at 4 weeks post-AAV injection are shown (scale bar is 100 μm). Western blot analysis of Chop (G), Bax (H) and Aat (I) in liver lysates from control and *Dhdds* LSKO mice, with β-Tubulin used as a loading control. (J) Western blot analysis of Aat in plasma from control and *Dhdds* LSKO mice, with Apoa1 used as a loading control. Representative western blots are shown. In panel (I), plasma was treated with an enzymatic deglycosylation kit (+) or sham (-) as control of the effect of glycosylation on protein mobility. "Aat Glyc": glycosylated (mature) Aat; "Aat Deglyc": deglycosylated Aat. (K) Densitometry analysis of plasma Aat relative to Apoa1 in control (blue) and *Dhdds* LSKO (red) mice. All data are presented as mean ± SD with significance determined by two-tailed student's t-test. n= 6 mice per group, n=3 in densitometry analysis. *p<0.05, **p<0.01, ***p<0.001 and ****p<0.001.

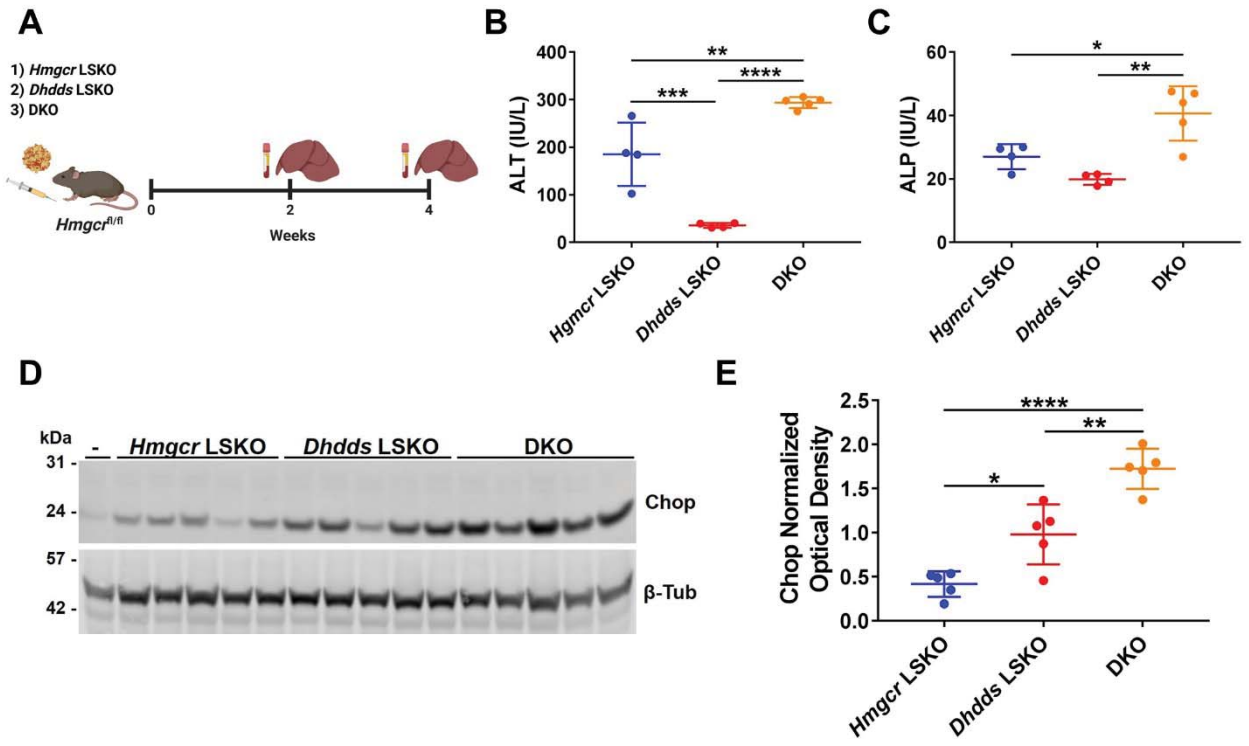

Figure 6. DKO mice show exacerbation of hepatocyte liver injury and ER stress. (A) 6 week old *Hmgcr*$^{fl/fl}$ mice were injected with 2 × 10^{11} GC of AAV-*Cre* and 5 × 10^{11} GC of AAV-CRISPR (DKO mice) and liver and plasma samples were collected at 2 and 4 weeks post-injection for analysis. 5 × 10^{11} GC of AAV-CRISPR-empty (no gRNA) or 2 × 10^{11} GC of AAV-GFP were included in the AAV dilutions respectively injected in *Hmgcr* LSKO and *Dhdds* LSKO mice, to deliver the same total AAV GC per mouse. ALT (B) and ALP (C) assay on plasma from *Hmgcr* LSKO, *Dhdds* LSKO and DKO mice at 2 weeks post-injection. (D) Western blot analysis of Chop in liver lysates from *Hmgcr* LSKO, *Dhdds* LSKO and DKO mice at 4 weeks post-injection, with β-Tubulin used as a loading control. "-": liver lysate from a *Hmgcr*$^{fl/fl}$ mouse used as negative control. Representative western blots are shown. (E) Densitometry analysis of Chop relative to β-Tubulin loading control. Data are shown as mean ± SD with significance determined by one-way ANOVA followed by Tukey test. n= 4 to 7 mice per group. *p<0.05, **p<0.01, ***p<0.001 and ****p<0.0001.